EAI Endorsed Transactions
on Context-aware Systems and Applications
Research Article EAI.EU

Fuzzy Logic Control Design and Implementation with DC-DC Boost Converter

Abdullah J. H. Al Gizi[1,*]

[1]Thi-Qar Technical College, Dept. Of Electromechanical Engineering , Southern Technical University, Iraq

Abstract

Being an electrical switch, this converter transforms an uncontrolled input DC voltage into a regulated one to get a desired output voltage. The MOSFET works in the circuit boost-converter as an electronic switch that closes and opens several times. The current passing through the inductor determines the modes operation of the boost-converter circuit. We proposed the new fuzzy control circuit (maximum power point (MPP) circuit using Fuzzy Logic Control (FLC) algorithm) was designed after replacing the DC source with a photovoltaic (PV) array and the duty cycle (constant) with the FLC and keeping the circuit components same except for the Pulses Width Modulation (PWM) of frequency 3800 Hz. In the full circuit, they controlled the MPP of the PV array through a boost converter and FLC., the relationship between the power and voltage of the PV array was drawn to access the MPP at fixed constant solar irradiance and temperature. The value of the solar irradiance altered during the day from low (in the morning) to high (with a peak at the noon) before being reduced to very low at the sunset. The proves that the FLC algorithm works efficiently to make the power of the PV cell always at the maximum value (MPP). The stability of the PV cell voltage and its current change also proves that it operates according to the specifications of the P-V and I-V characteristics of the PV cell referred to earlier the output voltage was increased because we used a step-up converter (boost converter with FLC). The achievement system is showed to be efficient and robust in improving solar charging and rectifying capacity.

Keywords: Boost-Converter, MPP, FLC, PV Array, MOSFET.

Received on 22 April 2022, accepted on 11 June 2022, published on 12 July 2022

doi: 10.4108/eetcasa.v8i24.1920

1. Introduction

Automation control systems are widespread in science and technology. The impact of global warming on global climate change has become clear. Where the weather has changed a lot and the global temperature has risen because of the amount of carbon dioxide emissions associated with the combustion of fossil fuels, where annually, 6.5 million people die due to air pollution [1]. Therefore, more research and experiments have been conducted on renewable energies such as (solar energy, in d energy, biomass energy, ideal energy, and geothermal energy), besides many other types[2], [1-6] predictable a change process that might recuperate the exhibition and reliability of the 2-axis solar hanger-on. It was talented into two phases, counting the hardware and software expansion. Automation regulator arrangements are extensive in discipline and ability. Computerization control arrangements are extensive in discipline and ability. The representative hardware expedient used in industrial regulator is Programmable-Logic-Controllers (PLC) that boards many industrial systems. PLC is oppressed to control plants or industrial equipment such as water and waste regulator, energy, oil and gas purifying [7].[8] Here, a novel topology baptized an ANFIS (Adaptive Neuro-Fuzzy Inference System) supervisor based soft swapped DC/DC converter with non-isolated joined inductor has been replicated and obtainable for refining the power of stand-alone PV system [9-13]. A Proportional-Integral (PI) founded Maximum-Power-Point-Tracking (MPPT) regulator procedure is projected in this study where it is practical to a Buck-Boost converter[14-21]. The additional style is when the present of

* Corresponding author. Email: abdullah.algizi@stu.edu.iq

the inductance in a period of time develops zero called intermittent disorder style (DCM)[22].So, the industrialized magnetic field in the coil stowed an energy that is relative to the creation of inductor and square current ($W=1/2\times L\times I^2$)[23, 24]. At last, a proper evaluation is recognized among the important types of DC-DC boost converters in terms of efficiency, number of components, and stability[25]. For this reason, a special kind of classical controller i.e. Type-III controller is introduced for obtaining better performance. This paper describes the designing of a Type-III controller for a dc-dc switched-mode boost converter.[9]. This paper presents the high gain boost converter in the concept of Switch Mode Power Supply (SMPS) DC/DC Circuit with proposed topology[26-28].We design of boost Converter with FLC controller and implemented. This proposal is based on synergistic mixture of fuzzy rules with Power-voltage characteristics of the PV array. The FLC controller is further designed to implementing the photovoltaic (PV) scheme. The entire structure is further adjusted by solar limits under numerous functioning settings to advance the solar presentation in rapports of accusing and correcting. The presentation of the projected analog-implemented MPP manager is assessed by interfacing it with photovoltaic (PV) system. FLC algorithm works very efficiently to make the power of the PV cell always at the maximum value (MPP) compared to the values in the MATLAB specifications for the PV cell used in this test system. Our paper organization as following, collected works review that has been done in the part"1" to clarify the difference of the manuscript with other papers, that it is innovative, it are used in the parts " 2 " to describe the results of research and results discussion & comparison with other related works in the parts "3,4 " to support the analysis of the our results that it is innovative in the section " 5".

2. Problem statement

2.1 Boost Converter Design and Implementation.

Being an electrical switch this converter transforms an uncontrolled input DC voltage into a regulated one to get a desired output voltage. It consists of electronic circuits with little energy loss when connected with two circuits for increasing or decreasing the input voltage displays the circuit diagram of a Boost-converter circuit. The values shown in the circuit were implemented in the MATLAB program. These are indicated for the sake of clarification, simplification ,and drawing various signals without any practical implication [15]

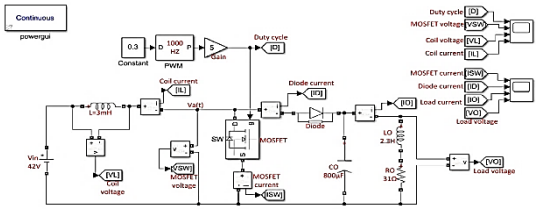

Figure 1. Boost converter circuit

2.2 Operation of Step-up Converter

The values of the circuit components are indicated on each element. The MOSFET works in this circuit as an electronic switch that closes and opens several times with the (PWM) frequency of 1000 Hz.

(a) shows the variation in the duty cycle wave (D), where (T_{on}) is the time at which the MOSFET closes (0.3 of the total time T), while (T_{off} is the time at which the MOSFET opens (0.7 of the total time T) with T = T_{on} + T_{off}. Being an electronic switch when the MOSFET is in on state Fig. (b)) it turns into short circuit and the voltage across it becomes zero ($V_a(t) = 0V$). They connect directly the inductor to the source (Vin = 42 V) for 0.3 T (Fig. (c)). The current in the inductor does not change momentarily, but depends on the time constant ($\tau = L / R$). The current continues to increase through the inductance during 0.3 T Fig. (d)) wherein the value is identical to the MOSFET current. The developed magnetic field in the coil stored an energy that is proportional to the product of inductance and square current ($W=1/2\times L\times I^2$)[23]

.

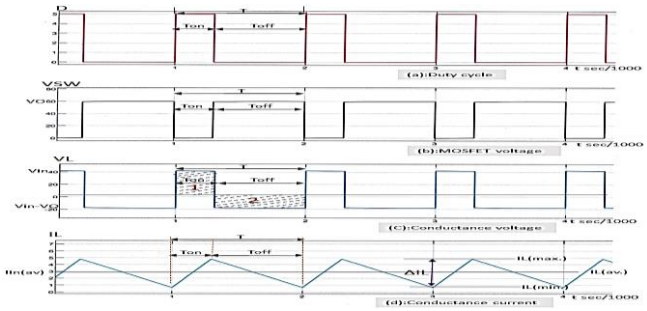

Figure 2. Variation in the (a) duty cycle, (b) MOSFET voltage, (c) conductor voltage, and (d) conductor current

Here, the diode is reverse biased (open circuit) because of the voltage $V_a(t) = 0V$. In the second stage (T_{off} = 0.7 T), the MOSFET is in the open circuit because the duty cycle amplitude = 0. Meanwhile, the diode is forward biased (closed circuit) and the coil becomes connected in series with the diode.

The linear converters (IC m317) are variable voltage regulator these types of converters lose the high power and energy. On the other hand, boost and back convertors operation depends on PWM technique the power losses are very low and the higher efficiency than the linear converters. These types of converters named synchronous converters because using MOSFIT (Low-side FET on resistance) instead of diode in parallel with series circuit of coil and capacitance to less the power lose, Use these types of converters with electrical cars . the circuit of synchronous converters is very simple so consist of dc power supply in sies with high-side FET and Low-side FET on resistance that connected in parallel with series circuit of coil and capacitance as shown in Fig 1.b if there is damage any parts of circuit will be replace by suitable correct parts .

At this moment the coil signal is inverted because the current remains in the same direction where the coil energy is discharged into the capacitor and the load over 0.7 T with the inductor voltage VL = Vin-VO = -18 V .Fig.1(c). The output voltage is the sum of the input and inductance voltages. This circuit acts as a step-up converter. During the open circuit of the MOSFET, the capacitive load (CO) is charged. When the diode is the open circuit, the capacitor is discharged through its load and the value of the output current remains constant depending on the value of the capacitance ((c)). The capacitive voltage is decreased and increased when the inductor is powered and discharged its energy, respectively ((d)) [29]. Following relationships are used to find the inductor and capacitor parameters in a boost converter.

$$L=\frac{V_{in}.D}{fs.\Delta IL}=\frac{V_O..(1-D).D}{fs.\Delta IL}=\frac{R_O.(1-D)}{fs.(\Delta IL/I_o)}=\frac{V_{in}.(V_O-V_{in}).D}{fs.\Delta IL.V_O}$$

$$I_{in(av.)}=I_{L(av.)}=\frac{I_{L(\max)}+I_{L(\min)}}{2} \quad (1)$$

Fig. 1(d) The output current was selected between 0.2 to 0.4 in order to estimate the value of the inductor ripple (ΔIL) [30].

$$\Delta IL=(0.2to0.4).I_o(\max).\frac{V_o}{V_{in}},\ C_o(\min)=.\frac{I_{o(\max)}.D}{fs.\Delta V_o} \quad (2)$$

where V_O = output voltage,= input V_{in} duty cycle, D = voltage, L = inductor, I_{in} = input current, ΔIL = estimated inductor ripple current , I_O = output current, fs = switching frequency, R_O = load resistance, $V_{in}(\min)$ = minimum input voltage,maximum input current, $I_{in}(\max)$ = $I_{in}(\min)$ = minimum input voltage,maximum $I_L(\max)$ = inductor current, $I_L(\min)$ = minimum inductor current, desired ΔV_o = minimum output capacitor, and $C_o(\min)$ = output ripple voltage.

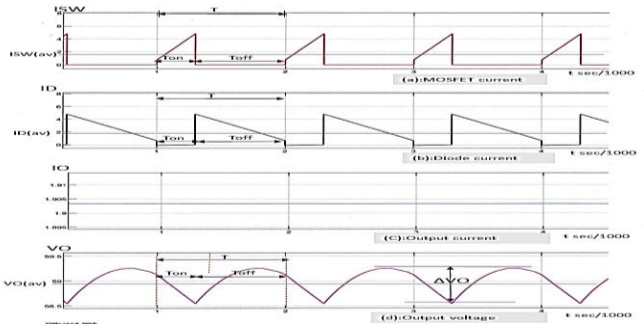

Figure 3. Variation in the (a) MOSFET current, (b) diode current, (c) output current, and (d) output voltage

2.3 Modes operation of step up DC to DC converter

The current passing through the inductor determines the modes operation of the boost-converter circuit. If the current always is not equal to zero, it is called in this case the continuous condition mode (CCM). The second mode is when the current of the inductor in a period of time becomes zero called discontinuous condition mode (DCM)[31]. For being suitable for use in high power and its good performance, the CCM will be adopt in this thesis d shows inductor current (IL) never reach zero. The current passing through the inductor changes according to the closing and opening of the MOSFET circuit, which makes the diode connected in series with the inductor also close and open the opposite of the MOSFET, which makes the inductor current vary with time.The voltage across the inductor when (t=Ton) equal to: -

$$T=T_{on}+T_{off} \quad (3)$$

$$T_{off}=T+T_{on}=T-DT=T(1-D) \quad (4)$$

$$\Delta i_L(off)=\frac{v_{in}-v_o}{L}T(1-D) \quad (5)$$

$$\Delta i_L(on)+\Delta i_L(off)=0\ [32].\frac{v_{in}}{L}DT=\frac{-v_{in}+v_o}{L}T(1-D)$$

, then $v_{in}D=(-v_{in}+v_o)(1-D)\ V_o=\frac{1_o}{1-D}V_{in}$ this is a proof of Equation To ensure that the boost converter works in a CCM, the value of the critical inductance (L_C) must be found. This is done when the value of L_c in is assumed to be zero. That is, the inductor has entered the DCM stage. Therefore, the value of the L_c should be the lowest required value.

The voltage across the inductor when (t=Ton) equal to: -

$T=T_{on}+T_{off}\ \ T_{off}=T-T_{on}=T-DT=T(1-D)\ \Rightarrow$

$$\Delta i_L(off)=\frac{v_{in}-v_o}{L}T(1-D) \quad (6)$$

$$\Delta i_L(on)+\Delta i_L(off)=0\ [32].\frac{v_{in}}{L}DT=\frac{-v_{in}+v_o}{L}T(1-D)$$

,then $v_{inD}=(-v_{in}+v_o)(1-D)$,$v_o=\frac{1}{1-D}v_{in}$ (7)

Calculating the critical value of the inductor L_c (in Eq.), Substitute values from 0 to 1 of the Duty Cycle(D) into the $D(1-D)^2$ term .Fig.1(a) MATLAB simulation to draw the relationship between the $D(1-D)^2$ function and the D values. When the value of D is equal to 1/3, the term is the greatest possible and is $D(1-D)^2$ equal to (0.1**48**) Fig. 1 (b). So$L_{c(min)} \geq \frac{D(1-D)^2 xR}{2xf_S}$. [32] In our case in, when the R=31Ω and the $f_S = 1000Hz$, the minimum value of the inductor is L= 2.3 mH. An inductor value of L= 3 mH was used, so the results were in the CCM.

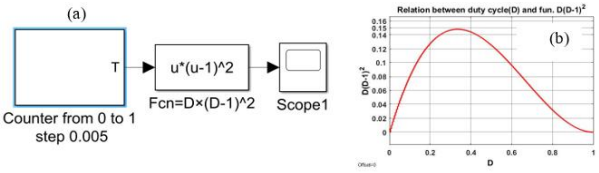

Figure 4. (a) MATLAB simulation for D(D-1)^2 function . (b) Relation between duty cycle and D(D-1) ^2 value

In order to calculate the value of the critical output capacitance (C_c), and going back to d, the lowest value of the capacitance is when the lowest voltage value reaches zero (V_c(min)=0). This happens when the capacitor is completely discharged before charging again in the second cycle.$V_{c(min)} = zero$ Where $V_c = V_o = \frac{\Delta V_c}{2} = \frac{\Delta V_o}{2} = 0$, the lowest value of output capacitor. $\Delta V_c = \frac{I_o}{C} DT = \frac{DI_O}{fc} = \frac{DI_O}{fc} = \frac{DV_O}{fCR}, V_O = \frac{\Delta V_O}{2} = \frac{DV_O}{2fCR}$ then, $C_C = \frac{D}{2fsR}$ same result in Equation. (8)

It is concluded from Equations and that the value of the inductor and the capacitor are inversely proportional to the value of the frequency, so a high frequency is chosen in order to reduce their size.

3. Boost Converter with PV Array and FLC

The new circuit (Fig. 5) was designed after replacing the DC source with a PV array (as specified in Table **I**) as well as the duty cycle (constant) with the FLC in Fig. 1 and keeping the circuit components same except for the PWM of frequency 3800 Hz, the Equations (1 to 9) were used for further calculations. In the full circuit, it controlled the MPP of the PV array through a boost converter and FLC. Fig. 6 shows the internal details of the FLC circuit. In Fig. 7, the relationship between the power and voltage of the PV array was drawn to access the MPP at fixed constant solar irradiance and temperature. The value of the solar irradiance altered during the day from low (in the morning) to high (with peak at the noon) before being reduced to very low at the sunset Fig. 9.

Table 1. Specifications of the proposed PV array

PV	Sanyo Electrical of Panasonic Group VBHN 220 AA 01
$P_{max.}$	220.759 W
$V_{O.C}$	52.3 V
$I_{S.C}$	5.35 A
V_{max}	42.7 V
I_{max}	5.17 A

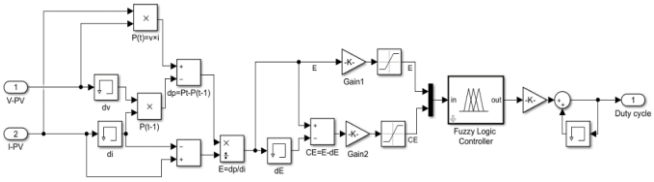

Figure 5. Design of the MPP circuit using FLC algorithm

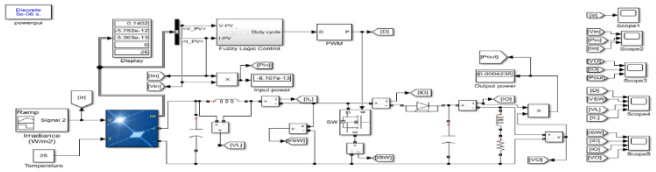

Figure 6. Circuit diagram of the FLC algorithm

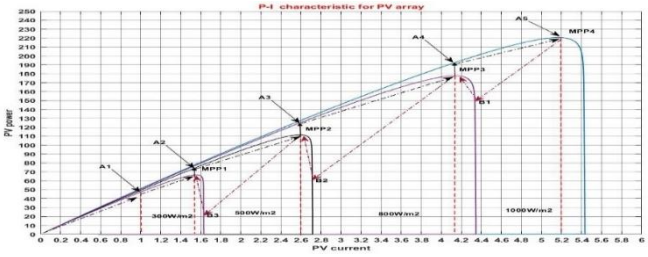

Figure 7. Power-voltage characteristics of the PV array

Figure represents the relationship between the current and power of the PV cell (The new circuit (Fig. 5) was designed after replacing the DC source with a PV array (as specified in Table I) as well as the duty cycle (constant) with the FLC in Fig. 1 and keeping the circuit components same except for the PWM of frequency 3800 Hz, the Equations (1 to 9) were used

for further calculations. In the full circuit, the MPP of the PV array was controlled through a boost converter and FLC. Fig. 6 shows the internal details of the FLC circuit. In Fig. 7, the relationship between the power and voltage of the PV array was drawn to access the MPP at fixed constant solar irradiance and temperature. In practice, the value of the solar irradiance altered during the day from low (in the morning) to high (with peak at the noon) before being reduced to very low at the sunset Fig. 9. Tables where different shapes were drawn at each solar irradiance (300, 500, 800 and 1000 W/m^2) using the MATLAB code as shown in Unlike the influence of the solar irradiance, the temperature was kept constant despite its effect on the efficiency variation of the PV cell. To avoid the complications, a constant temperature of 25 °C was chosen for the PV cell and maintained the same throughout the experiment. Four MPP values for each solar irradiance level were determined. Furthermore, it was assumed that the solar irradiance started at zero and the power as well as the current was also zero until the point reached to A1 where the solar irradiance stabilized at 300 W/m^2 till MPP1. Where, ΔI is the change in current, I(t) and I(t-1) are the currents at time t and (t-1), respectively, Other symbols have their usual meaning.The error was found to be always negative to the right of the MPP while positive to the left of it. In addition, the value of the error represented the amount of distance of the point from the MPP. However, the change of error was negative or positive depending on the direction of the point from the MPP as its signal signified the direction of movement in either way of the MPP or reversing its direction depending on the type of converter used. The value showed the speed of movement of the point. The following shows the values got from of the studied PV array Table I in which the voltage change was fixed at 2 V and power was varied according to different location of the point. The results in clearly showed the robustness of the using the Fuzzy rules for setting up the entire experiment. In the current study, the two inputs of FLC formed known crisp values (change in power and voltage) and the fuzzifcation was performed for these values by converting them into the linguistic values. From point A1, the FLC compared the value of error and change of error based on the 49 fuzzy rules. The power and current of the PV cell were selected as the crisp inputs for the FLC. Table shown the incoming signals were converted to the linguistic variables where 7 variables (called linguistic values) were selected for both inputs and output as Negative Big NB, Negative Medium (NM), Negative Small (NS), Zero (ZE), Positive Small (PS), Positive Medium (PM), and Positive Big (PB).Enlists the linguistic values of the duty cycle (D) according to which the voltage or current of the PV array was decreased or increased. For example, when E was NS and CE was PB then the duty cycle was NS. This implied that when the error was negative and small (i.e. to the right of the MPP and close to it) as well as the change of error was positive and large (i.e. it moved against the MPP quickly) then it was needed to return the point to the MPP by lowering the value of D by a tiny negative amount, the Equations and were used to determine the value of D through its relation with current and voltages (as decreasing the value of D). In Region 1, both the error and the change of error were negative. This implied that the point to the right of the MPP was moved towards it because the current in this region changed very little compared to the power. Thus, any amount of D was not required because that could make the point turn to the left of the MPP wherein the previous amount was sufficient to reach MPP. In Region 2 (on the right of MPP), the change of error was positive, which implied that the point moved against the direction of the MPP.Therefore, an amount of D was required depending on the amount of the error (E) and change of error (CE). Likewise, Region 3 and 4 were prepared. Due to zero error for the rules 22, 23, 27 and 28, it was impossible to know whether the point is to the right or the left of the MPP, making a possibility to switch between them. Eventually, the point was moved from A1 to MPP1 to A2, and so on to MPP4 when the solar radiation altered each time from lower to higher , respectively. Conversely, when the solar radiation changed from top to bottom, the point moved from MPP4 to B1 to MPP3 and then down to A1 before being reached to zero. The point did not move in the paths rather it moved randomly to the left or right of the MPP when the solar radiation changed. Owing to its non-linear nature, the variation of many factors affected the PV array such as temperature, solar radiation, load current (change in resistance) and others. Fig. shows a membership function which was part of the fuzzy inference engine and comprised the first input (c)). The boundaries of the membership function were defined carefully by measuring the input signal before connecting the FLC. Then, a gain was added in order to raise or lower for adjusting the values later, getting a satisfactory result. For the output, it was delta D (ΔD) and thus the output boundary was chosen to be small in order to ensure that the step amount becomes small. Because of tiny range (between zero and one), the value of duty cycle was divided into 100 parts. For example, each time a part of 100 was added or subtracted to the previous value depending on the location of the point from the MPP. If the D was divided into a tiny amount, reaching MPP took a long time. Conversely, for an enormous amount of division, the stability was lost and it swung around the MPP, making the system unstable. Thus, a gain was needed at the output to set the value.

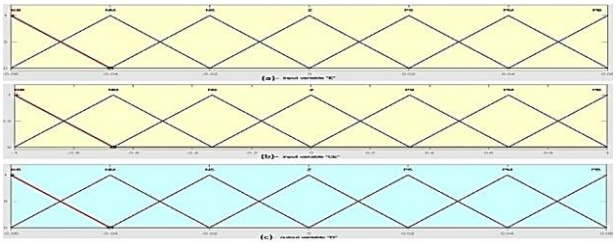

Figure 8. Membership functions for the variable (a) input (E), (b) input (CE), and (c) output (D)

Membership functions (MFs) are the structure blocks of fuzzy set philosophy, i.e., fuzziness in a fuzzy set is strongminded by its MF. So, the forms of MFs are significant for a specific problem meanwhile they consequence on a

fuzzy implication scheme. They may have dissimilar shapes like three-sided, trapezoidal, Gaussian, etc. The only disorder a MF necessity actually content is that it must vary between 0 and 1. A trapezoidal change hurries for a 3rd of the time of the change, travels at max haste for a 3rd of the period, then slows for a 3rd of a period. While a triangular change hurries for half the change then slows for the additional half. A trapezoidal change uses a higher hastening while a triangular change usages a higher max haste. So we neeeds higher max rapidity respone of our sytem.

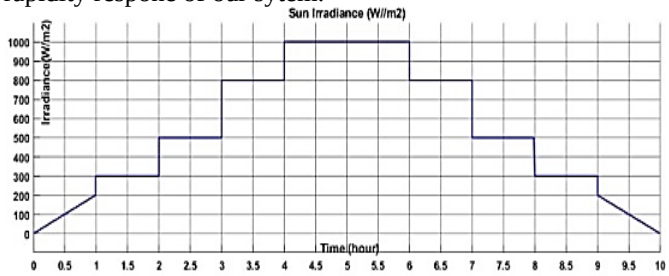

Figure 9. Solar irradiance

4. Results of boost converter and its efficiency

The boost converter circuit with the component values shown in was tested by MATLAB simulation, and different values of the duty cycle with Switching Frequency 1000Hz to test the circuit's efficiency shows the efficiency of the boost converter at a constant input voltage of 20 volts and a duty cycle (0.2, 0.3, 0.4, 0.5). All Fig.s show the input and output voltages and currents for each Duty Cycle. The efficiency values ranged up to 96% because the electronic parts used in the simulation are ideal without loss because the internal resistors of the components are not included.

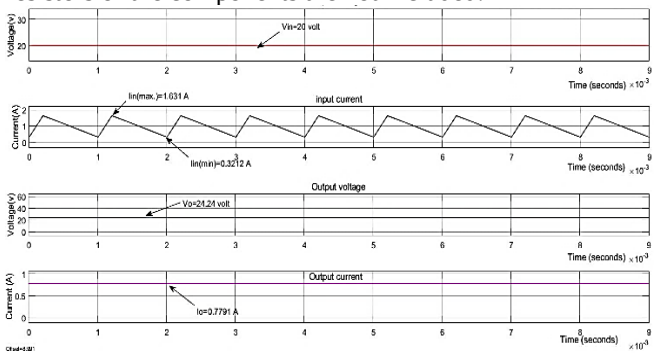

Figure 10. Input and output current and voltage for boost converter at D=0.2

Fig.10:Input and output current and voltage for boost converter at D=0.2 Simulation results for boost converter for different values for Duty Cycle shows the values of the boost converter for the practical circuit shown in Fig. 1 together with the values of the components. In the Simulation circuit, a switching frequency of 3550 Hz was used because the inductor used is 680 µH, according to Equation, the minimum frequency that can be used to make the buck converter in a CCM is 3270 Hz.

Table 2. Description of the fuzzy rules

CE / E	NB	NM	NS	ZE	PS	PM	PB
NB	1 ZE	2 ZE	3 ZE	4 NB	5 NB	6 NB	7 NB
NM	8 ZE	9 ZE	10 ZE	11 NM	12 NM	13 NM	14 NM
NS	15 ZE	16 ZE	17 ZE	18 NS	19 NS	20 NS	21 NS
ZE	22 NS	23 NS	24 ZE	25 ZE	26 ZE	27 PS	28 PS
PS	29 PS	30 PS	31 PS	32 PS	33 ZE	34 ZE	35 ZE
PM	36 PM	37 PM	38 PM	39 PM	40 ZE	41 ZE	42 ZE
PB	43 PB	44 PB	45 PB	46 PB	47 ZE	48 ZE	49 ZE

The efficiency of the practical circuit was lower than that of the simulation circuit in MATLAB for two reasons. The first is that the practical components have internal resistances that cause a loss of power, and the second is that the utilized factor of the boost converter is efficient in the first third of the values of the Duty Cycle according to Equation, where a &b shows the scheme of the utilized factor of the boost converter[23, 33, 34] [35, 36].WE can recuperate the efficiency of the practical circuit by decreasing the internal resistances of practical components . In variance to the boost converter, the buck converter works jobwise with the high values of the Duty Cycle.

$$U_f = \frac{1-D}{\sqrt{D}+\sqrt{1-D}} \qquad [23](9)$$

Where : U_f is a utilized factor , D is a Duty Cycle.

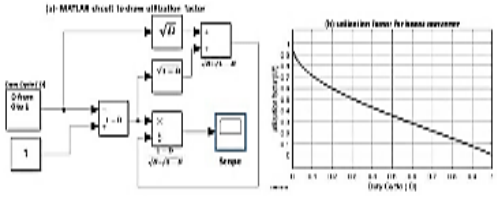

Figure 11. (a)- MATLAB circuit to draw the utilization factor . (b)- Utilization factor for boost converter

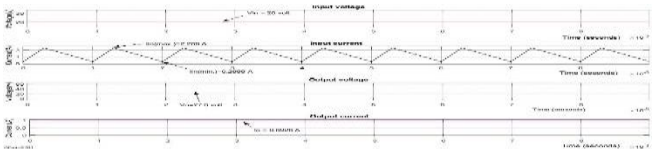

Figure 12. Input and output current and voltage for boost converter at D=0.3

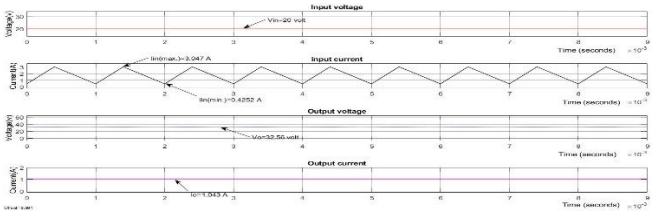

Figure 13. Input and output current and voltage for boost converter at D=0.4

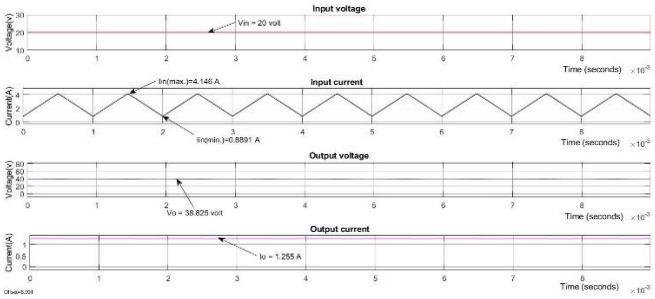

Figure 14. Input and output current and voltage for boost converter at D=0.5

5. Results of boost converter with PV Array and FLC discussion and compares with the findings of the previous studies

During the MATLAB experiment, the power of the PV cell was at the maximum value of each amount of solar radiation, as shown in 15 b. The value of the PV cell voltage was approximately altered at a constant rate while they increased the power with the increase in current. This proves that the FLC algorithm works efficiently to make the power of the PV cell always at the maximum value (MPP) compared to the values in the MATLAB specifications for the PV cell used in this experiment. The stability of the PV cell voltage and its current change also proves that it operates according to the specifications of the P-V and I-V features of the PV cell referred to earlier. shows that the output power was the maximum, and the output voltage was increased because we used a step-up converter. The battery voltage of the static PV is a slight bit slighter than that of the 1A-3P PV temporarily the power generation of the static PV is less than the 1A-3P PV, while the planned boost converter contrast with overall approaches gives an enhancement of MPPT compares with the findings of the previous studies[37-44]. In dissimilarity to the boost converter, the buck converter works jobwise with the high values of the Duty Cycle, i.e. in the preceding 3rd, meanwhile the use subject of the Buck Converter is the source of the Duty Cycle as compares with the previous studies.A first comparison yields a maximum mean nonconformity of very small amid experimental results and numerical imitation. The chief sources of errors are recognized, and enhancements are projected for improved model accuracy. The novelty of the plan stands in modeling the multiple-usage life cycle situation to support the reparability of the electronic device founded on a modular project of boost converters.[45-48] [49].

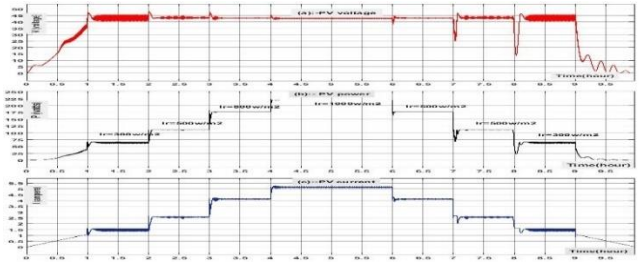

Figure 15. PV array (a) voltage, (b) power, and (c) current

Table 3. Actual values of V, P, ΔP, ΔV, E and CE for the studied PV array

No.	Point	Row no.	P(t)-P(t-1)	V(t)-V(t-1)	ΔP	ΔV	E	CE
1	MPP to A	3	219-220	44-42	-1	2	-1/2	
2	A to B	3	200-2019	46-44	-19	2	-19/2	-19/2+1/2=-18/2
3	B to C	3	160-200	48-46	-40	2	-40/2	-40/2+19/2=-21/2
4	C to D	3	100-160	50-48	-60	2	-60/2	-60/2+40/2=-20/2
5	D to E	3	10-100	52-50	-90	2	-90/2	-90/2+60/2=-30/2
6	E to D	4	100-10	50-52	90	-2	-90/2	
7	D to C	4	160-100	48-50	60	-2	-60/2	-60/2+90/2=30/2
8	C to B	4	200-160	46-48	40	-2	-40/2	-40/2+60/2=20/2
9	B to A	4	219-200	44-46	19	-2	-19/2	-19/2+40/2=21/2
10	A to MPP	4	220-219	42-44	1	-2	-1/2	-1/2+19/2=18/2
11	J to I	1	184-172	34-32	12	2	12/2	
12	I to H	1	195-184	36-34	11	2	11/2	11/2-12/2=-1/2
13	H to G	1	205-195	38-36	10	2	10/2	10/2-11/2=-1/2
14	G to F	1	215-205	40-38	10	2	10/2	10/2-10/2=0
15	F to MPP	1	220-215	42-40	5	2	5/2	5/2-10/2=-5/2
16	MPP to F	2	215-220	40-42	-5	-2	5/2	
17	F to G	2	205-215	38-40	-10	-2	10/2	10/2-5/2=5/2
18	G to H	2	195-205	36-38	-10	-2	10/2	10/2-10/2=0
19	H to I	2	184-195	34-36	-11	-2	11/2	11/2-10/2=1/2
20	I to J	2	172-184	32-34	-12	-2	12/2	12/2-11/2=1/2

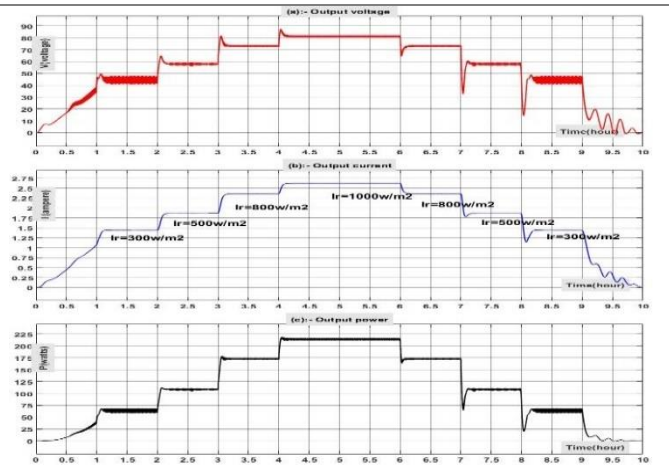

Figure 16. (a) output voltage, (b) output current, and (c) output power

Table 4. Simulation results for boost converter for different values for Duty Cycle

Duty Cycle	Vin (V)	$I_{in}=\frac{I_{in}(max)+I_{in}(min)}{2}$ (A)	Pin (W)	Vout (V)	Iout (A)	Pout (W)	% Efficiency
20%	20	= 0.9761	19.52	24.24	0.779	18.88	96.73
30%	20	= 1.28445	25.689	27.8	0.8926	24.81	96.59
40%	20	= 1.7361	34.722	32.56	1.043	33.96	97.8
50%	20	= 2.51755	50.351	38.825	1.255	48.72	96.77

6. Conclusion

The results of boost Converter test will be displayed without connecting them to the controller or the PV cell to know their efficiency and comparing the MATLAB simulation results with practical experiments results After that, the same boost converter circuits are tested, but with the controllers and with the PV. In the third stage, the results of merging the boost converter circuits are presented. The boost converter circuit with the component values was tested by MATLAB simulation, and different values of the Duty Cycle with Switching Frequency 1000Hz to test the circuit's efficiency. The efficiency values ranged up to 96% because the electronic parts used in the simulation are ideal without loss because the internal resistors of the components are not included. The efficiency of the practical circuit was lower than that of the simulation circuit in MATLAB for two reasons. The first is that the practical components have internal resistances that cause a loss of power, and the second is that the used factor of the boost converter is efficient in the first third of the values of the Duty Cycle .During the MATLAB experiment, the power of the PV cell was at the maximum value of each amount of solar radiation. The value of the PV cell voltage was approximately altered at a constant rate while the power was increased with the increase in current. This proves that the FLC algorithm works efficiently to make the power of the PV cell always at the maximum value (MPP) compared to the values in the MATLAB specifications for the PV cell used in this experiment.

References

[1] K. Salah-ddine, "Design and Modeling of DC/ DC Boost Converter for Mobile Device Applications," 05/02 2013.

[2] J. Caro, J. M. Ramirez, F. Peng, and A. Valderrabano-Gonzalez, "A DC–DC multilevel boost converter," *IET Power Electronics*, vol. 3, 11/12 2008, doi: 10.1049/iet-pel.2008.0253.

[3] A. Garrigós, D. Marroquí, A. García, J. M. Blanes, and R. Gutiérrez, "Interleaved, switched-inductor, multi-phase, multi-device DC/DC boost converter for non-isolated and high conversion ratio fuel cell applications," *International Journal of Hydrogen Energy*, vol. 44, no. 25, pp. 12783-12792, 2019/05/17/ 2019, doi: https://doi.org/10.1016/j.ijhydene.2018.11.094.

[4] F. Akar, "A fuel-cell/battery hybrid DC backup power system via a new high step-up three port converter," *International Journal of Hydrogen Energy*, vol. 46, no. 73, pp. 36398-36414, 2021/10/22/ 2021, doi: https://doi.org/10.1016/j.ijhydene.2021.08.130.

[5] R. Madhana and G. Mani, "Power enhancement methods of renewable energy resources using multiport DC-DC converter: A technical review," *Sustainable Computing: Informatics and Systems*, vol. 35, p. 100689, 2022/09/01/ 2022, doi: https://doi.org/10.1016/j.suscom.2022.100689.

[6] Y. Huangfu, Y. Ma, H. Bai, L. Xu, A. Wang, and R. Ma, "A family of high gain fuel cell front-end converters with low input current ripple for PEMFC power conditioning systems," *International Journal of Hydrogen Energy*, vol. 46, no. 53, pp. 27156-27172, 2021/08/03/ 2021, doi: https://doi.org/10.1016/j.ijhydene.2021.05.174.

[7] "Front Matter," in *Power Electronics Handbook (Fourth Edition)*, M. H. Rashid Ed.: Butterworth-Heinemann, 2018, pp. i-ii.

[8] V. Gandhi, S. V, and L. R, "Topological review and analysis of DC-DC boost converters," *Journal of Engineering Science and Technology*, vol. 12, pp. 1541-1567, 06/01 2017.

[9] A. Ghosh and S. Banerjee, "Design of Type-III controller for dc-dc switch-mode boost converter," in *2014 6th IEEE Power India International Conference (PIICON)*, 2014: IEEE, pp. 1-6.

[10] F. L. Luo and H. Ye, *Essential DC/DC Converters*. Taylor & Francis, 2006.

[11] L. Ashok Kumar, S. Albert Alexander, and M. Rajendran, "Chapter 5 - DC–DC converter topologies for solar PV," in *Power Electronic Converters for Solar Photovoltaic Systems*, L. Ashok Kumar, S. Albert Alexander, and M. Rajendran Eds.: Academic Press, 2021, pp. 207-234.

[12] L. Ashok Kumar, S. Albert Alexander, and M. Rajendran, "Chapter 7 - Emerging DC–DC converter topologies," in *Power Electronic Converters for Solar Photovoltaic Systems*, L. Ashok Kumar, S. Albert Alexander, and M. Rajendran Eds.: Academic Press, 2021, pp. 289-329.

[13] L. Ashok Kumar, S. Albert Alexander, and M. Rajendran, "Chapter 6 - Control of DC–DC converters," in *Power Electronic Converters for Solar Photovoltaic Systems*, L. Ashok Kumar, S. Albert Alexander, and M. Rajendran Eds.: Academic Press, 2021, pp. 235-288.

[14] "Preface," in *Switch-Mode Power Converters*, K. C. Wu Ed. Oxford: Academic Press, 2006, pp. xiii-xv.

[15] U. Yilmaz, A. Kircay, and S. Borekci, "PV system fuzzy logic MPPT method and PI control as a charge controller," *Renewable and Sustainable Energy Reviews*, vol. 81, pp. 994-1001, 2018/01/01/ 2018, doi: https://doi.org/10.1016/j.rser.2017.08.048.

[16] R. Bisht and A. Sikander, "An improved method based on fuzzy logic with beta parameter for PV MPPT system," *Optik*, vol. 259, p. 168939, 2022/06/01/ 2022, doi: https://doi.org/10.1016/j.ijleo.2022.168939.

[17] F. J. Vivas, F. Segura, J. M. Andújar, A. J. Calderón, and F. Isorna, "Battery-based storage systems in high voltage-DC bus microgrids. A real-time charging algorithm to improve the microgrid performance," *Journal of Energy Storage*, vol. 48, p. 103935, 2022/04/01/ 2022, doi: https://doi.org/10.1016/j.est.2021.103935.

[18] Z. Hu, H. Norouzi, M. Jiang, S. Dadfar, and T. Kashiwagi, "Novel hybrid modified krill herd algorithm and fuzzy controller based MPPT to optimally tune the member functions for PV system in the three-phase grid-connected mode," *ISA Transactions*, 2022/02/12/ 2022, doi: https://doi.org/10.1016/j.isatra.2022.02.009.

[19] Y. Singh and N. Pal, "Reinforcement learning with fuzzified reward approach for MPPT control of PV systems," *Sustainable Energy Technologies and Assessments*, vol. 48, p. 101665, 2021/12/01/ 2021, doi: https://doi.org/10.1016/j.seta.2021.101665.

[20] A. Abubakar, C. F. M. Almeida, and M. Gemignani, "Review of Artificial Intelligence-Based Failure Detection and Diagnosis Methods for Solar Photovoltaic Systems," *Machines*, vol. 9, no. 12, p. 328, 2021. [Online]. Available: https://www.mdpi.com/2075-1702/9/12/328.

[21] B.-J. Huang, Y.-C. Huang, G.-Y. Chen, P.-C. Hsu, and K. Li, "Improving Solar PV System Efficiency Using One-Axis 3-Position Sun Tracking," *Energy Procedia*, vol. 33, pp. 280-287, 2013/01/01/ 2013, doi: https://doi.org/10.1016/j.egypro.2013.05.069.

[22] S. M. Sousa, L. S. Gusman, T. A. S. Lopes, H. A. Pereira, and J. M. S. Callegari, "MPPT algorithm in single loop current-mode control applied to dc–dc converters with input current source characteristics," *International Journal of Electrical Power & Energy Systems*, vol. 138, p. 107909, 2022/06/01/ 2022, doi: https://doi.org/10.1016/j.ijepes.2021.107909.

[23] M. Barrenetxea Iñarra, I. Baraia-Etxaburu Zubiaurre, I. Larrazabal Bengoetxea, and I. Zubimendi Azaceta, "Power electronic converter design handbook," 2018.

[24] N. Smith and R. McCann, "Analysis and simulation of a multiple input interleaved boost converter for renewable energy applications," in *2014 IEEE 36th International Telecommunications Energy Conference (INTELEC)*, 2014: IEEE, pp. 1-7.

[25] V. I. Gandhi, V. Subramaniyaswamy, and R. Logesh, "Topological review and analysis of DC-DC boost converters," *J. Eng. Sci. Technol*, vol. 12, pp. 1541-1567, 2017.

[26] J. Wang, B. Wang, L. Zhang, J. Wang, N. I. Shchurov, and B. V. Malozyomov, "Review of Bidirectional DC-DC Converter Topologies for Hybrid Energy Storage System of New Energy Vehicles," *Green Energy and Intelligent Transportation*, p. 100010, 2022/05/20/ 2022, doi: https://doi.org/10.1016/j.geits.2022.100010.

[27] H. Sorouri, M. Sedighizadeh, A. Oshnoei, and R. Khezri, "An intelligent adaptive control of DC–DC power buck converters," *International Journal of Electrical Power & Energy Systems*, vol. 141, p. 108099, 2022/10/01/ 2022, doi: https://doi.org/10.1016/j.ijepes.2022.108099.

[28] Q. Su, C. Li, X. Guo, X. Zhang, and J. Li, "Robust fault diagnosis for DC–DC Boost converters via switched systems," *Control Engineering Practice*, vol. 112, p. 104836, 2021/07/01/ 2021, doi: https://doi.org/10.1016/j.conengprac.2021.104836.

[29] W. Shepherd and L. Zhang, *Power converter circuits*. CRC Press, 2004.

[30] T. Instruments, "Basic calculation of a boost converter's Power Stage," *Application Report SLVA327B*, 2009.

[31] B. Abdessamad, K. Salah-Ddine, and C. E. Mohamed, "Design and Modeling of DC/DC Boost Converter for Mobile Device Applications," *International Journal of Science and Technology*, vol. 2, no. 5, pp. 394-401, 2013.

[32] K.-H. Chao, C. Tseng, H. Huang, and G. Liu, "Design and implementation of a bidirectional DC-DC converter for stand-alone photovoltaic systems," *energy*, vol. 4, p. 8, 2013.

[33] R. Dermouche, A. Talaoubrid, L. Barazane, Y. Sellami, M. Tadjine, and N. Zioui, "Qualitative and quantitative analysis of the reliability of NPC and ANPC power converters for aeronautical applications," *Alexandria Engineering Journal*, vol. 61, no. 6, pp. 4863-4873, 2022/06/01/ 2022, doi: https://doi.org/10.1016/j.aej.2021.09.056.

[34] J. Divya Navamani, A. Lavanya, D. Almakhles, and M. Jagabar Sathik, "A review on segregation of various high gain converter configurations for distributed energy sources," *Alexandria Engineering Journal*, vol. 61, no. 1, pp. 675-700, 2022/01/01/ 2022, doi: https://doi.org/10.1016/j.aej.2021.06.026.

[35] S. Bacha, I. Munteanu, and A. I. Bratcu, "Power electronic converters modeling and control," *Advanced textbooks in control and signal processing*, vol. 454, no. 454, 2014.

[36] A. Emadi, A. Khaligh, Z. Nie, and Y. J. Lee, *Integrated power electronic converters and digital control*. CRC Press, 2017.

[37] Y. Zhong *et al.*, "A review on the GaN-on-Si power electronic devices," *Fundamental Research*, vol. 2, no. 3, pp. 462-475, 2022/05/01/ 2022, doi: https://doi.org/10.1016/j.fmre.2021.11.028.

[38] "Front-matter," in *Power Electronics Device Applications of Diamond Semiconductors*, S. Koizumi, H. Umezawa, J. Pernot, and M. Suzuki Eds.: Woodhead Publishing, 2018, pp. i-iii.

[39] "Copyright," in *Power Electronics Device Applications of Diamond Semiconductors*, S. Koizumi, H. Umezawa, J. Pernot, and M. Suzuki Eds.: Woodhead Publishing, 2018, p. iv.

[40] J. Achard *et al.*, "List of Contributors," in *Power Electronics Device Applications of Diamond Semiconductors*, S. Koizumi, H. Umezawa, J. Pernot, and M. Suzuki Eds.: Woodhead Publishing, 2018, pp. xi-xiii.

[41] "Copyright," in *Wide Bandgap Power Semiconductor Packaging*, K. Suganuma Ed.: Woodhead Publishing, 2018, p. iv.

[42] "Front Matter," in *Wide Bandgap Power Semiconductor Packaging*, K. Suganuma Ed.: Woodhead Publishing, 2018, pp. i-iii.

[43] T. Aichinger *et al.*, "List of contributors," in *Wide Bandgap Power Semiconductor Packaging*, K. Suganuma Ed.: Woodhead Publishing, 2018, pp. ix-x.

[44] U. Radhakrishna, "Chapter Seven - Physics-based III-Nitride device modeling," in *Semiconductors and Semimetals*, vol. 102, R. Chu and K. Shinohara Eds.: Elsevier, 2019, pp. 243-306.

[45] M. Rio, K. Khannoussi, J.-C. Crebier, and Y. Lembeye, "Addressing Circularity to Product Designers: Application to a Multi-Cell Power Electronics Converter," *Procedia CIRP*, vol. 91, pp. 134-139, 2020/01/01/ 2020, doi: https://doi.org/10.1016/j.procir.2020.02.158.

[46] Z. Zhang, R. Pittini, M. A. E. Andersen, and O. C. Thomsena, "A Review and Design of Power Electronics Converters for Fuel Cell Hybrid System Applications," *Energy Procedia*, vol. 20, pp. 301-310, 2012/01/01/ 2012, doi: https://doi.org/10.1016/j.egypro.2012.03.030.

[47] P. K. Maroti, S. Padmanaban, M. S. Bhaskar, V. K. Ramachandaramurthy, and F. Blaabjerg, "The state-of-the-art of power electronics converters configurations in electric vehicle technologies," *Power Electronic Devices and Components*, vol. 1, p. 100001, 2022/03/01/ 2022, doi: https://doi.org/10.1016/j.pedc.2021.100001.

[48] M. Moustaid, V. Platel, M. Guillet, H. Reynes, and C. Buttay, "Modeling and test of a thermosyphon loop for the cooling of a megawatt-range power electronics converter," *International Journal of Thermofluids*, vol. 13, p. 100129, 2022/02/01/ 2022, doi: https://doi.org/10.1016/j.ijft.2021.100129.

[49] N. Mohan, T. M. Undeland, and W. P. Robbins, *Power electronics: converters, applications, and design*. John wiley & sons, 2003.